Available online at www.sciencedirect.com
SCIENCE DIRECT
Journal of Catalysis 241 (2006) 211–220
JOURNAL OF CATALYSIS
www.elsevier.com/locate/jcat

Characterization and catalytic properties of Sn-modified rapidly quenched skeletal Ni catalysts in aqueous-phase reforming of ethylene glycol

Fuzhong Xie [a], Xianwen Chu [a], Huarong Hu [a], Minghua Qiao [a,*], Shirun Yan [a], Yuanlong Zhu [a], Heyong He [a], Kangnian Fan [a,*], Hexing Li [b], Baoning Zong [c], Xiaoxin Zhang [c]

[a] *Department of Chemistry and Shanghai Key Laboratory of Molecular Catalysis and Innovative Materials, Fudan University, Shanghai 200433, P.R. China*
[b] *Department of Chemistry, Shanghai Normal University, Shanghai 200234, P.R. China*
[c] *Research Institute of Petroleum Processing, Beijing 100083, P.R. China*

Received 25 January 2006; revised 28 April 2006; accepted 1 May 2006

Abstract

Skeletal Ni (RQ Ni) catalyst was prepared by alkali leaching of rapidly quenched $Ni_{50}Al_{50}$ alloy. By impregnating RQ Ni with $SnCl_4$ followed by thermal treatment in inert atmosphere, homogeneous Sn-modified skeletal Ni (RQ Ni–Sn) catalysts were obtained. It was found that thermal treatment induces alloying of the deposited metallic Sn with Ni, forming Ni_3Sn alloy segregated on the catalyst surface. In aqueous-phase reforming of ethylene glycol, the RQ Ni catalyst was less selective in producing H_2 but more selective in producing alkanes than the Raney Ni catalyst described in the literature. This is attributed to the expansion of the lattice of RQ Ni favoring the dissociation of CO and, consequently, the methanation reaction consuming H_2. Moreover, the structural difference influences the reaction pathway, with the undesired C–O cleavage pathway obstructed on RQ Ni. Modification of RQ Ni with Sn drastically improves the H_2 selectivity. On the RQ $Ni_{80}Sn_{20}$ catalyst, alkane production was virtually retarded, whereas H_2 selectivity as high as 98 mol% was achieved at high conversion. Based on the characterizations and previous findings, it is suggested that Sn may block the active sites for CO adsorption and/or dissociation, thus suppressing the undesired methanation reaction. On the other hand, bifunctional Ni–Sn ensembles may form, in which Sn facilitates H_2O dissociation while neighboring Ni adsorbs CO, thus promoting the desired water–gas shift reaction, leading to more H_2.

Keywords: Skeletal Ni; Rapid quenching; Sn modification; Aqueous-phase reforming; Ethylene glycol; H_2 production

1. Introduction

H_2 is considered a potential source of clean energy because it does not emit greenhouse gases after direct combustion or use in a H_2 fuel cell. The current industrialized methods for H_2 production are based mainly on nonrenewable fossil fuels [1–4]; thus H_2 from renewable sources is highly desirable.

Recently, Dumesic and coworkers [5–13] demonstrated that H_2 can be produced from sugars and sugar alcohols (derived from biomass) at temperatures near 500 K in a single-reactor aqueous-phase reforming (APR) process, and that the selectivity for H_2 increases significantly when hydrocarbons have a C:O stoichiometry of 1:1 and a H_2 content relative to carbon >1. Their results indicate that catalytic APR of glucose, sorbitol, glycerol, and ethylene glycol is feasible in generating H_2-rich fuel gas. In addition, the APR process is energy saving, because vaporization of water and the hydrocarbons is not required. An even more attractive property is that the water–gas shift (WGS) reaction is thermodynamically favored at the low temperatures of APR, which can lead to lower CO content in H_2 than that achieved in steam reforming processes.

Several types of catalysts have been designed for the APR process, including the supported Pt catalysts [5–8,11], SiO_2-supported metal catalysts [8], and Sn-modified Raney Ni catalysts [9–12]. Among these, the Pt/Al_2O_3 catalyst and the Sn-modified Raney Ni catalyst are the most promising. The high H_2 selectivity from the reforming of ethylene glycol can be achieved over the Pt/Al_2O_3 catalyst [5,6], whereas the addition

* Corresponding authors. Fax: +86 21 65642978.
E-mail addresses: mhqiao@fudan.edu.cn (M.H. Qiao), knfan@fudan.edu.cn (K.N. Fan).

0021-9517/$ – see front matter
doi:10.1016/j.jcat.2006.05.001

of Sn is necessary to avoid alkane formation by the methanation reaction over Raney Ni [9–12]. Although the Pt/Al_2O_3 catalyst is more active in terms of specific activity, the Sn-modified Raney Ni catalyst is less expensive, making it economically more competitive than the former in the APR of ethylene glycol, a sustainable feedstock derived from biomass, sugars, and sugar-alcohols [8]. Moreover, because Raney Ni is metallic, it exhibits higher thermal conductivity compared with oxide-supported reforming catalysts, which is crucial to the startup and transient response of the reformer [14].

In this paper, we extend the scope of the APR catalysts to the rapidly quenched skeletal Ni catalyst (designated RQ Ni) prepared by alkali leaching of the rapidly quenched $Ni_{50}Al_{50}$ alloy (Ni/Al, w/w, designated RQ $Ni_{50}Al_{50}$). It is noted that the Raney Ni catalyst is leached from the naturally solidified $Ni_{50}Al_{50}$ alloy. We reported previously that the RQ Ni catalyst behaves differently in the hydrogenation of unsaturated organic compounds compared with the Raney Ni catalyst irrespective of their similar compositions, and attributed the underlying cause to their discrepancies in textural and structural properties [15]. Thus, it will be interesting to explore the performance of the RQ Ni catalyst in the APR of ethylene glycol. In contrast, the Sn-modified Ni catalysts, either supported or unsupported, are usually prepared by surface reaction of organotin compounds (e.g., $Sn(C_4H_9)_3OAc$ [9–12], $Sn(CH_3)_4$ [16–18], $Sn(n\text{-}C_4H_9)_4$ [19–21]) with Ni preadsorbed with hydrogen or in hydrogen atmosphere. Here we used the less hazardous and inexpensive $SnCl_4$ and a simple impregnation procedure to deposit Sn on the RQ Ni catalyst (designated RQ Ni–Sn). The effects of Sn on the texture and structure of the RQ Ni catalyst were investigated in detail. The catalytic behaviors of the RQ Ni–Sn catalysts in APR of ethylene glycol were correlated and discussed based on the characterizations.

2. Experimental

2.1. Catalyst preparation

The RQ $Ni_{50}Al_{50}$ alloy was prepared by a single-roller melt-spinning technique. A mixture containing equal weights of metallic Ni and Al of >99.9% purity was melted at 1573 K in an induction furnace for sufficient time to ensure homogeneity of the melt. The ribbon (ca. 5 mm wide and 20 μm thick) was fabricated by spraying the melt on a water-cooled high-speed rotating copper wheel with a cooling rate of ca. 10^7 $K\,s^{-1}$. The alloy was subsequently ground, and the fraction of 100–200 mesh was used throughout the experiments.

The RQ Ni–Sn catalysts were prepared as described below. Under gentle stirring, 1 g of the RQ $Ni_{50}Al_{50}$ alloy was added to the NaOH aqueous solution (10 mL, 6.0 M) at 363 K. After addition, the mixture was stirred at 363 K for 1 h, to achieve further alkali leaching. The black powder was washed free of alkali with distilled water. The as-prepared RQ Ni catalyst was then soaked in 11 mL of ethanol solution containing a desired amount of $SnCl_4$ and stirred gently for 1 h at 303 K. The nominal Sn/Ni molar ratios were 1/99, 2/98, 5/95, 10/90, and 20/80 for the catalysts labeled RQ $Ni_{99}Sn_1$, RQ $Ni_{98}Sn_2$, RQ $Ni_{95}Sn_5$, RQ $Ni_{90}Sn_{10}$, and RQ $Ni_{80}Sn_{20}$, respectively. The resulting RQ Ni–Sn catalysts were washed with distilled water until free of chlorine ions and kept in water before activity testing.

For characterizations, the RQ Ni and RQ Ni–Sn catalysts were also washed with ethanol to replace water and finally stored in ethanol. All of the measurements were made within 24 h of catalyst preparation. Because the catalysts are pyrophoric, care must be taken to avoid air oxidation during sample handling.

2.2. Catalyst characterization

Because the melting point of metallic Sn is as low as 505 K and the APR of ethylene glycol is usually conducted below 543 K, before characterization, the RQ Ni and RQ Ni–Sn catalysts were subjected to thermal treatment at 543 K under inert atmosphere for at least 1 h. The bulk compositions of the catalysts were determined by inductively coupled plasma-atomic emission spectroscopy (ICP-AES), using a Hitachi P-4010 instrument, after total dissolution in aqua regia. Their morphologies were observed by scanning electron microscopy (SEM), using a Philips XL30 microscope. Sn distribution was obtained on an energy-dispersive X-ray emission analyzer (EDX) attached to the SEM apparatus.

The nitrogen isotherms and subsequent BET surface areas (S_{BET}) and pore distributions were measured by N_2 adsorption at 77 K on a Micromeritics TriStar3000 apparatus. The catalyst was transferred to the adsorption glass tube with the storage liquid and pretreated at 543 K under N_2 (99.9995%) flow for 2 h. It was weighed by difference in the adsorption tube on completion of the measurement.

Powder X-ray diffraction (XRD) was executed on a Bruker AXS D8 Advance X-ray diffractometer using Cu-K_α radiation (0.15418 nm), at a tube voltage of 40 kV and a current of 40 mA. Catalyst with solvent was heated in the hot stage to 543 K for 1 h, cooled to room temperature, and detected. All of the operations were shielded by Ar (99.9995%) flow.

X-ray photoelectron spectroscopy (XPS) was performed on a Perkin-Elmer PHI5000C instrument to determine the surface electronic states and surface composition of the catalysts. After being treated at 543 K under N_2 (99.9995%) flow for 1 h, the catalyst was immersed in ethanol, pressed into a self-supported disc, and mounted on the sample plate. It was degassed in the pretreatment chamber for 2 h at 383 K in vacuo before being transferred to the analyzing chamber, in which the background pressure was $<2 \times 10^{-9}$ Torr. All of the binding energy (BE) values were obtained after the surface oxides were removed by Ar ion sputtering and were referenced to the C 1s peak of contaminant carbon at 284.6 eV with an uncertainty of ±0.2 eV.

H_2 temperature-programmed desorption (H_2-TPD) profiles were obtained in the following manner. After the catalyst was treated at 543 K for 1 h under Ar flow (99.9995%, deoxygenated by an Alltech Oxy-trap filter), it was cooled to room temperature before saturation chemisorption of H_2 by pulsed injection, as confirmed by the constant eluted peak area monitored with a thermal conductivity detector (TCD). The maxi-

mum desorption temperature, 850 K, was achieved at a ramp rate of 20 K min^{-1}. The catalyst was weighed after being cooled to room temperature. The active surface area (S_H) was calculated from the total volume of H_2 desorbed by assuming an equal distribution of atoms among the (100), (110), and (111) planes of Ni and a H/Ni stoichiometry of unity.

2.3. Activity test and product analysis

The reactor system for the APR of ethylene glycol was established according to the setup described by Shabaker et al. [7]. The as-prepared RQ Ni or RQ Ni–Sn catalyst with water was loaded in the stainless steel tubular reactor (6 mm i.d.). No additional activation step of the catalysts was executed except for the thermal treatment at 543 K for 1 h under Ar (99.9995%) flow. An aqueous solution containing 5 wt% ethylene glycol was fed to the reactor in an up-flow configuration. Ar was used to regulate the system pressure. The reforming was typically conducted with a catalyst mass of 0.5 g, a liquid hourly space velocity (LHSV; volumetric flow rate of feed solution/catalyst bed volume) of 3.60 h^{-1}, a temperature of 498 K, and a system pressure of 2.58 MPa, unless otherwise specified. The reaction course was monitored by sampling the gas and liquid products at intervals, followed by gas chromatography (GC) analysis. For the gas effluent, hydrogen, carbon monoxide, methane, and carbon dioxide were separated by a 5-Å molecular sieve packed column and evaluated by a TCD. Methane, ethane, and propane were separated by a Porapak R packed column and examined by a flame ionization detector (FID). The liquid products, including methanol, ethanol, acetone, 2-propanol, and ethylene glycol, were separated by an HP-5 capillary column and examined by the FID. The liquid products were also qualified by gas chromatography–mass spectroscopy (Finnigan Voyager) with an HP-5 capillary column. According to Shabaker et al. [10], H_2 selectivity is defined as

$$\begin{aligned}&H_2 \text{ selectivity } (\%)\\ &\quad = (\text{moles of } H_2 \text{ produced/moles of C in gas phase})\\ &\qquad \times (5/2) \times 100, \end{aligned} \tag{1}$$

which takes into account the WGS reaction, and alkane selectivity is defined as

$$\begin{aligned}&\text{Alkane selectivity } (\%)\\ &\quad = (\text{mol of C in gaseous alkanes}\\ &\qquad /\text{total mol of C in gas products}) \times 100. \end{aligned} \tag{2}$$

It should be noted that according to the definitions, the summation of H_2 selectivity and alkane selectivity does not lead to unity, because they are calculated based on independent hydrogen and carbon balances, respectively.

3. Results

3.1. Bulk composition and texture

The bulk composition, BET surface area, pore volume, and mean pore diameter of the RQ Ni and RQ Ni–Sn catalysts are summarized in Table 1. Chemical analysis shows that the addition of more $SnCl_4$ during preparation increased the amount of Sn incorporated in the RQ Ni–Sn catalysts accordingly. However, the relative ratio of Sn between the amount in the resulting catalyst and the nominal amount kept decreasing from 98 to 41% when the nominal Sn/Ni molar ratio was increased from 1/99 to 20/80. On the other hand, the BET surface areas of the catalysts first increased marginally at a nominal Sn/Ni ratio < 5/95, then decreased slightly at higher Sn/Ni ratios, consistent with the finding that the BET surface areas of the Raney Ni–Sn catalysts did not change significantly when tributyl tin acetate was used as the Sn source [10]. Table 1 also shows that the mean pore diameter and pore volume increased monotonously with respect to Sn/Ni ratio.

Table 1
Physicochemical properties of the RQ Ni and RQ Ni–Sn catalysts

Catalyst	Bulk composition (atomic ratio)	S_{BET} ($m^2\,g^{-1}$)	V_{pore} ($cm^3\,g^{-1}$)	d_{pore} (nm)	S_H ($m^2\,g^{-1}$)
RQ Ni	$Ni_{79.8}Al_{20.2}$	77	0.092	4.7	14.3
RQ $Ni_{99}Sn_1$	$Ni_{79.2}Sn_{0.8}Al_{20.0}$	77	0.095	4.9	12.0
RQ $Ni_{98}Sn_2$	$Ni_{78.8}Sn_{1.4}Al_{19.8}$	78	0.107	5.0	11.9
RQ $Ni_{95}Sn_5$	$Ni_{76.8}Sn_{3.4}Al_{19.8}$	79	0.112	5.7	11.4
RQ $Ni_{90}Sn_{10}$	$Ni_{74.8}Sn_{6.1}Al_{19.1}$	73	0.119	6.4	10.6
RQ $Ni_{80}Sn_{20}$	$Ni_{71.2}Sn_{11.2}Al_{17.6}$	71	0.137	7.9	10.0

Fig. 1 shows the SEM images and EDX results for the RQ $Ni_{99}Sn_1$ catalyst. Note that the morphologies of the RQ Ni and RQ Ni–Sn catalysts are similar. Fig. 1a shows that the RQ $Ni_{99}Sn_1$ catalyst has a relatively flat surface and a rough cross-section, likely inherited from the ribbon-like morphology of the pristine RQ $Ni_{50}Al_{50}$ alloy. Fig. 1b shows that unlike the smooth surface of the RQ $Ni_{50}Al_{50}$ ribbon (not shown), the surface of the leached catalyst is highly fragmentized. The cross-sectional images (Figs. 1a and c) clearly demonstrate that the RQ $Ni_{99}Sn_1$ particle is composed of even smaller secondary particles (diameter ca. 2 μm). These secondary particles have round contours, in sharp contrast to the angular morphologies of Raney Ni [15]. The addition of Sn decreased the dimensions of the secondary particles; for the RQ $Ni_{80}Sn_{20}$ catalyst, the size of the secondary particles was ca. 1 μm. It is possible that the acidic $SnCl_4$ solution dissolved additional residual metallic Al and Ni from RQ Ni, leading to further fracturing of the secondary particles.

EDX experiments were performed to investigate the distribution of Sn in the RQ Ni–Sn catalysts. A typical result is shown in Fig. 1d, demonstrating that the evolution of the Sn concentration closely follows that of the Ni concentration, indicating the homogeneity of the distribution of Sn associated with Ni. Sn was also uniformly dispersed on the RQ $Ni_{80}Sn_{20}$ catalyst with the highest Sn content studied here. This verifies that the present $SnCl_4$-impregnation method is a promising alternative for the preparation of homogeneous Sn-modified Ni catalyst.

3.2. Phase composition

Before being treated at 543 K in Ar atmosphere, all of the RQ Ni and RQ Ni–Sn catalysts had XRD patterns similar to that of fcc Ni, but with a slightly broadened peak width at higher Sn content. No Sn-related phase emerged, implying the homo-

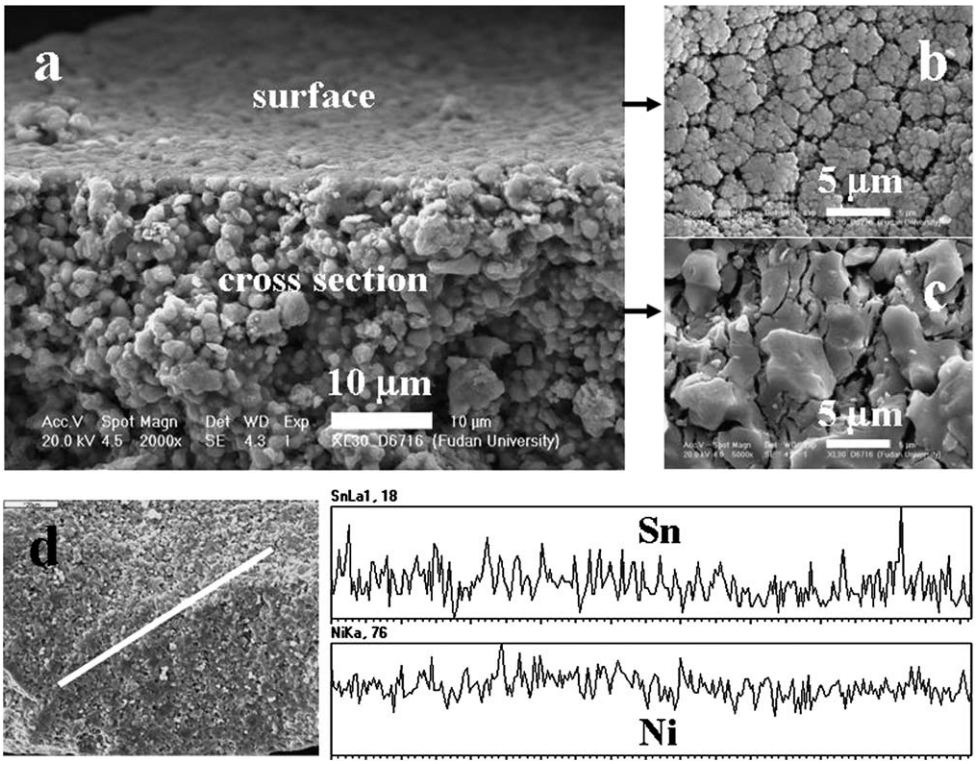

Fig. 1. (a) SEM image of the RQ $Ni_{99}Sn_1$ catalyst, and the corresponding surface (b) and cross-sectional images (c). (d) X-Ray line profiles of Ni and Sn in the RQ $Ni_{99}Sn_1$ catalyst. The line drawn on (d) denotes the range being scanned.

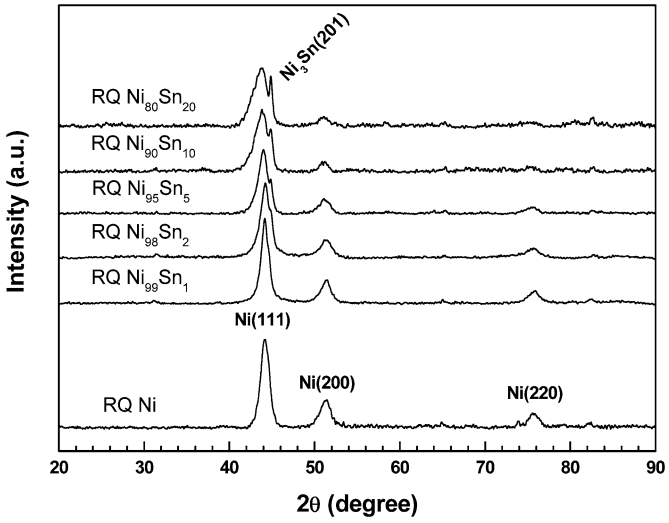

Fig. 2. XRD patterns of the RQ Ni and RQ Ni–Sn catalysts with different Sn contents.

geneous dispersion and extremely small crystallite size of the deposited metallic Sn. Thermal treatment noticeably changed the XRD patterns. As shown in Fig. 2, all catalysts exhibited diffractions at 2θ of 44.2, 51.4, and 75.7°, corresponding to the (111), (200), and (220) planes of fcc Ni, respectively [22]. Broadening of the Ni(111) peak was also observed with the increment of Sn. It is noteworthy that the unit-cell parameter of fcc Ni derived from these Bragg angles was ∼0.3551 nm, larger than the values for Ni crystal (0.35238 nm) [23] and Raney Ni (0.3528–0.3535 nm) [24]. The lattice expansion of the skeletal Ni catalyst has been linked to the more confined relaxation of the Ni atoms in the $Ni_{50}Al_{50}$ alloy at a faster cooling rate [15]. An alternative explanation may be that the lattice expansion results from the defects introduced by rapid quenching. Recent atomically resolved STM images of surface defects on Ru(0001) have shown regions with lattice expansion of up to 10% in the immediate vicinity of the defects [25]. Because these two situations have the same origin, distinguishing between them can be difficult.

Besides the features arising from fcc Ni, the intensity of the shoulder peak at 2θ of 44.8° was developed at higher Sn content, attributable to the (201) diffraction of hexagonal Ni_3Sn [22] due to alloying between metallic Ni and Sn during thermal treatment. Thus, the asymmetric tail at the lower side of the Ni(111) diffraction for the RQ Ni–Sn catalysts, which also gained in intensity at higher Sn content, can be assigned to the (002) diffraction of hexagonal Ni_3Sn. The formation of Ni–Sn alloys at 543 K was not unexpected; Onda et al. obtained Ni–Sn alloys using chemical vapor deposition of $Sn(CH_3)_4$ on Ni/SiO_2 at 448 K [17].

3.3. Surface composition

Fig. 3 illustrates the XPS spectra of the Ni 2p and Sn 3d levels for the RQ Ni and RQ Ni–Sn catalysts. Fig. 3a shows only one Ni $2p_{3/2}$ peak at 852.7 eV assignable to metallic Ni [26]. There is essentially no oxidized nickel species on these catalysts, consistent with the observations of Fouilloux [27] and Delannay et al. [28] on Raney Ni. In contrast, Fig. 3b reveals two chemical states of Sn after curve fitting: metallic Sn, with

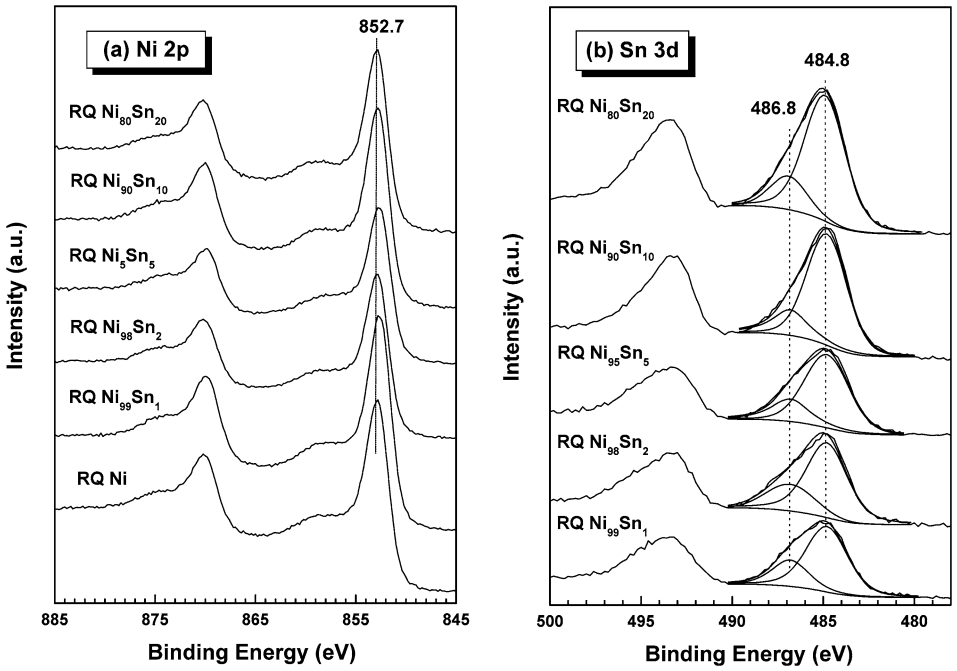

Fig. 3. XPS spectra of (a) Ni 2p and (b) Sn 3d levels of the RQ Ni and RQ Ni–Sn catalysts.

Table 2
Surface compositions of the RQ Ni–Sn catalysts determined by XPS

Catalyst	Sn/Ni (mol%)		$Sn^0/(Sn^0+Sn^{\delta+})$[a] (mol%)
	Bulk	Surface	
RQ $Ni_{99}Sn_1$	1.0	4.3	73
RQ $Ni_{98}Sn_2$	1.8	6.8	74
RQ $Ni_{95}Sn_5$	4.4	7.4	75
RQ $Ni_{90}Sn_{10}$	8.2	8.5	78
RQ $Ni_{80}Sn_{20}$	15.7	10.3	81

[a] $Sn^{\delta+}$ represents Sn^{4+} or Sn^{2+} which cannot be differentiated by XPS.

a Sn $3d_{5/2}$ BE of 484.8 eV, and oxidized tin species (Sn^{4+} or Sn^{2+}), with a Sn $3d_{5/2}$ BE of 486.8 eV [26], with >70% of Sn in the metallic state (Table 2).

Table 2 compares the bulk and surface Sn/Ni ratios in the RQ Ni–Sn catalysts and shows that the surface Sn/Ni ratio increased with the bulk one, with the former exceeding the latter for the catalysts with Sn/Ni nominal ratios <10/90. At higher Sn/Ni nominal ratios, the increase in surface Sn/Ni ratio became less evident. For RQ $Ni_{80}Sn_{20}$, the surface Sn/Ni ratio was even lower than the bulk one. Because, based on the argument that metallic Sn has much lower surface energy (710 mJ m^{-2}) than Ni (2450 mJ m^{-2}) [29], the surface enrichment of Sn itself was not applicable for the lower surface Sn/Ni ratio than the bulk one for RQ $Ni_{80}Sn_{20}$, the Ni_3Sn alloy was most likely segregated on the catalyst surface in the form of island-like crystallites. It is anticipated that the higher the Sn content, the larger the Ni_3Sn crystallites, and thus the portion of Sn beyond the detection depth of the XPS technique is increased. This interpretation can satisfactorily account for the evolution of the surface Sn/Ni ratios in Table 2.

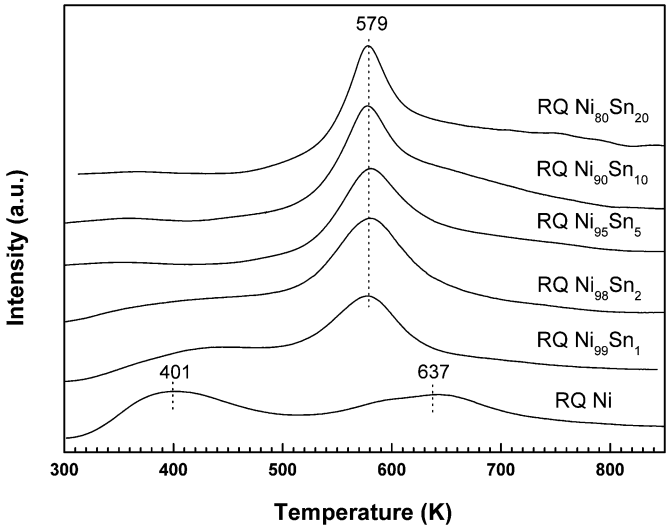

Fig. 4. H_2-TPD features of the RQ Ni and RQ Ni–Sn catalysts.

3.4. Surface sites

To obtain the dependence of surface active sites on Sn content, H_2-TPD profiles were acquired; these are plotted in Fig. 4. Fig. 4 shows that RQ Ni was characterized by two hydrogen desorption maxima at ca. 401 and 637 K, indicating the presence of at least two kinds of active sites. Because the low-temperature peak occurred in a temperature range similar to that on Ni single crystals with low Miller indices [30], following Arai et al. [31], we ascribe this to hydrogen chemisorbed on low-Miller index planes of RQ Ni. On the other hand, the high-temperature peak, which was dominant on RQ Ni treated at lower temperature [15], can be assigned to defects or lattice expansion. This assignment is in agreement with the theoretical

calculation of Greeley et al., who identified that surface expansion can noticeably improve the stability of surface hydrogen on the Ni(111) surface [32]. It is conceivable that thermal treatment at high temperature removes some defects, as evidenced by the sharpened diffractions compared with the freshly prepared RQ Ni, leading to the appearance of the low-temperature peak.

Fig. 4 shows that after Sn modification, the low-temperature peak was attenuated gradually and became indiscernible when the nominal Sn/Ni ratio was 5/95. The reduced number of desorption peaks suggests that the active sites over the RQ Ni–Sn catalysts became more uniform, which may have decreased the adsorption modes of the reactant and suppressed side reactions. At the first sight, considering that Sn itself does not adsorb hydrogen and that the amount of hydrogen adsorbed on the Ni_3Sn alloy is at least one order of magnitude lower than that adsorbed on Ni [18], it appears that Sn or Ni_3Sn preferentially blocked the low-Miller index planes on RQ Ni, leaving the adsorption sites for high-temperature hydrogen intact. However, it was found that S_H decreased only slightly after Sn modification (Table 1); thus, we can also assume that more defects were generated during Sn modification, as can be inferred from the broadened Ni(111) diffraction in Fig. 2 and the smaller particle size found on SEM. On the other hand, the loss of hydrogen due to Sn occupation can be partly compensated for by the newly generated defects and also may be impeded by the clustering of Ni_3Sn on the catalyst surface, as suggested by XPS.

3.5. Aqueous-phase reforming of ethylene glycol

3.5.1. Comparison between RQ Ni and Raney Ni

Before addressing the effect of Sn on the RQ Ni catalyst in the APR of ethylene glycol to H_2, we compared RQ Ni with Raney Ni to elucidate the effect of rapid quenching on catalytic performance. We found that the carbon balance was within 10% for the catalytic runs.

Table 3 compiles the H_2 and alkane selectivities, and gas and liquid product distributions, at 498 and 538 K over the RQ Ni and the previously reported Raney Ni catalysts [10]. The table shows that RQ Ni exhibited comparable or lower H_2 selectivity and higher alkane selectivity than Raney Ni. However, it is noteworthy that the RQ Ni catalyst produced less CO in the outlet gas, below the detection limit of 50 ppm. This result is significant especially in the field of H_2 fuel cells, considering that the anode materials are usually vulnerable to CO poisoning [33]. Based on the increased alkane concentrations in the gas products, we propose that CO depletion on the RQ Ni catalyst occurred mainly due to the enhanced activity in the methanation or Fischer–Tropsch (F-T) reaction rather than in the WGS reaction.

As for the liquid products, Table 3 shows that the RQ Ni catalyst favored formation of lower-alcohol methanol rather than ethanol, especially at high temperature. Shabaker et al. [10] reported that methanol is a desirable product because it contains a C–O linkage and may be further reformed to H_2 at high yields. For comparison, ethanol is preferred on Raney Ni particularly at low temperature. No acetic acid, acetaldehyde, or glycolaldehyde (the main liquid byproducts on Raney Ni) was identified in the liquid products when RQ Ni was used as the catalyst. Acetic acid is known to be troublesome due to its high stability in aqueous solution [10] and corrosivity [12]. Moreover, reforming of these liquid byproducts cannot be carried out with high H_2 selectivity, because methane is generated concurrently [10]. Instead, a small amount of 2-propanol and acetone were obtained over RQ Ni, with the latter being the dehydrogenation product of the former. Shorthouse et al. [34] identified selective dehydrogenation of 2-propanol to acetone as the major reaction pathway on the Ni(111) surface, and also reported that acetone desorption competes very effectively with unselective decomposition to smaller species.

Table 3
Comparison of the catalytic behaviors of RQ Ni and Raney Ni in APR of 5 wt% ethylene glycol solution

	Raney Ni [10]	RQ Ni[a]	Raney Ni [10]	RQ Ni[a]
Temperature (K)	498	498	538	538
Pressure (MPa)	2.58	2.58	5.13	5.13
LHSV (h^{-1})	4.13	3.60	8.26	3.60
Conversion of C to gas (%)	97	92	104	102
H_2 selectivity (%)	35	35	28	21
Alkane selectivity (%)	44	47	47	59
Gas products (mol%)				
H_2	47.6	47.4	41.4	34.9
CO_2	30.4	30.8	31.9	27.2
CO	0.02	n.d.[b]	0.03	n.d.[b]
Methane	20.7	22.8	25.6	36.4
Ethane	0.97	1.12	0.92	1.43
Propane	0.28	0.23	0.18	0.15
Butane	0.02	0.00	0.01	0.00
Liquid products (mol%, excluding unreacted EG)				
Methanol	10.2	85.1	34.3	95.1
Ethanol	48.3	12.9	2.5	3.5
Acetic acid	30.2	0.0	63.2	0.0
Acetaldehyde	7.3	0.0	0.0	0.0
Glycolaldehyde	4.0	0.0	0.0	0.0
2-Propanol	0.0	0.2	0.0	0.2
Acetone	0.0	1.8	0.0	1.2

[a] 0.5 g of catalyst.
[b] Below the detection limit.

3.5.2. The effect of Sn

Fig. 5 shows the evolutions of H_2 and alkane selectivities against the amount of Sn incorporated in the bulk of the RQ Ni catalyst. Similar to the promoting effect of Sn on Raney Ni [9,10], the selectivity to H_2 increased when the Sn content increased in the RQ Ni–Sn catalysts. As shown, a bulk Sn/Ni ratio as low as 1.0 mol% was sufficient to improve the H_2 selectivity from 35% on RQ Ni to 54% on RQ $Ni_{99}Sn_1$. H_2 selectivity exceeded 90% when the bulk Sn/Ni ratio was >4.4%. Meanwhile, alkane selectivity followed an opposite trend to that of H_2; on RQ $Ni_{80}Sn_{20}$, alkane selectivity was <1%, whereas H_2 selectivity reached as high as 98%.

Although Sn modification led to similar changes in H_2 and alkane selectivities on RQ Ni and Raney Ni, the kinetic data compiled in Table 4 suggest that the modification mechanisms were not the same for these two catalysts. The presence of transport limitations under the reaction conditions specified in

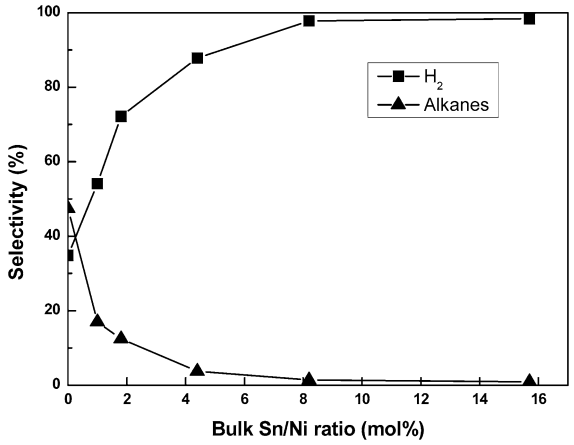

Fig. 5. Effect of bulk Sn/Ni molar ratio of the RQ Ni and RQ Ni–Sn catalysts on the H_2 and alkane selectivities in APR of ethylene glycol. Reaction conditions: 0.5 g of catalyst, 5 wt% of ethylene glycol aqueous solution, LHSV of 3.60 h^{-1}, temperature of 498 K, and pressure of 2.58 MPa.

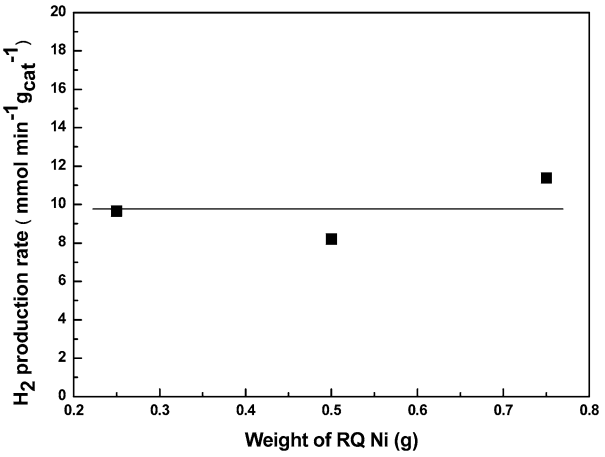

Fig. 6. H_2 production rate per gram of catalyst as a function of the weight of RQ Ni used in APR of ethylene glycol. Reaction conditions: 5 wt% of ethylene glycol aqueous solution, LHSV of 22.6 h^{-1}, temperature of 498 K, and pressure of 2.58 MPa.

Table 4 was tested following the method proposed by Koros and Nowak [35]. It has been claimed that the reaction rate per gram of catalyst is proportional to S, the number of active sites per unit volume of the reactor, in the absence of any transport limitations. Thus, for the skeletal Ni catalysts, the reaction rate per gram of catalyst should remain constant at various catalyst weights in the kinetically controlled regime. As shown in Fig. 6, the H_2 production rates per gram of catalyst are almost identical irrespective of the weight of RQ Ni used, strongly indicating that the data in Table 4 are intrinsic. According to Shabaker et al. [10], for the Raney Ni–Sn catalysts, the turnover frequencies (TOFs) of the alkanes decreased due to the addition of Sn, whereas the TOFs of H_2 were nearly unaffected. For the present RQ Ni–Sn catalysts, Table 4 reveals that aside from the decrement of the TOFs of the alkanes, the TOFs of H_2 and CO_2 increased steadily with the addition of Sn. It is also noted that the TOFs as well as the H_2 production rates over the RQ Ni and RQ Ni–Sn catalysts are lower than those over the Raney Ni and Raney Ni–Sn catalysts [10]. However, the deviations are generally within one order of magnitude and may be due to the experimental differences among laboratories.

Fig. 7 compares the effects of system pressure on H_2 and alkane selectivities over the RQ Ni and RQ $Ni_{80}Sn_{20}$ catalysts. The reaction temperature and the LHSV of ethylene glycol were maintained at 498 K and 3.6 h^{-1}. For RQ Ni, when the pressure was increased from 2.58 to 3.62 MPa, H_2 selectivity dropped

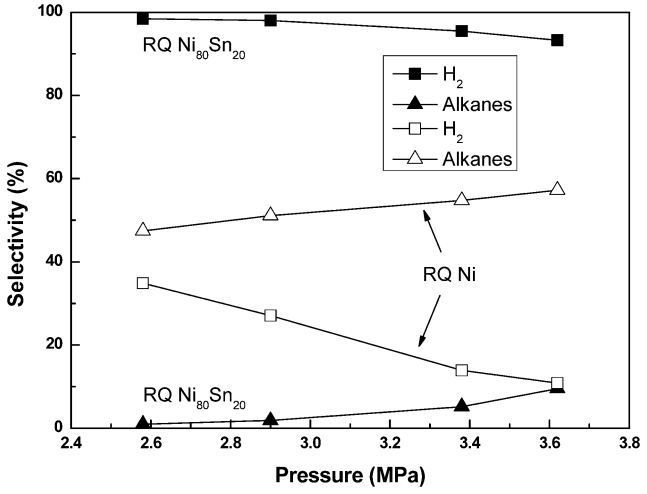

Fig. 7. Effect of system pressure on the H_2 and alkane selectivities for APR of ethylene glycol over the RQ Ni and RQ $Ni_{80}Sn_{20}$ catalysts. Other reaction conditions: 0.5 g of catalyst, 5 wt% of ethylene glycol aqueous solution, LHSV of 3.60 h^{-1}, and temperature of 498 K. Conversion is above 90% for all points.

from 35 to 11% and alkane selectivity rose from 47 to 57%. Although the H_2 and alkane selectivities on the RQ $Ni_{80}Sn_{20}$ catalyst evolved similarly to those on RQ Ni, the extents of the changes were less remarkable; the H_2 selectivities were always >90%, and the alkane selectivities were well below 10%, demonstrating that RQ $Ni_{80}Sn_{20}$ is a H_2-specific catalyst even

Table 4
The H_2 and alkane selectivities and the reaction rates over the RQ Ni and RQ Ni–Sn catalysts in APR of ethylene glycol[a]

Catalyst	Conversion of C to gas (%)	TOF (min^{-1})					H_2 production ($\mu mol\,cm^{-3}$ reactor min^{-1})
		H_2	CO_2	CH_4	C_2H_6	C_3H_8	
RQ Ni	11.8	0.22	0.16	0.159	0.0069	0.0021	21
RQ $Ni_{99}Sn_1$	9.6	0.33	0.17	0.130	0.0053	0.0002	28
RQ $Ni_{98}Sn_2$	7.8	0.41	0.19	0.061	0.0021	0	33
RQ $Ni_{95}Sn_5$	7.6	0.64	0.24	0.013	0	0	51
RQ $Ni_{90}Sn_{10}$	7.5	0.72	0.26	0.005	0	0	54
RQ $Ni_{80}Sn_{20}$	7.1	0.77	0.27	0	0	0	57

[a] Reaction conditions: 0.5 g of catalyst, 5 wt% of ethylene glycol aqueous solution, LHSV of 22.6 h^{-1}, temperature of 498 K, and pressure of 2.58 MPa.

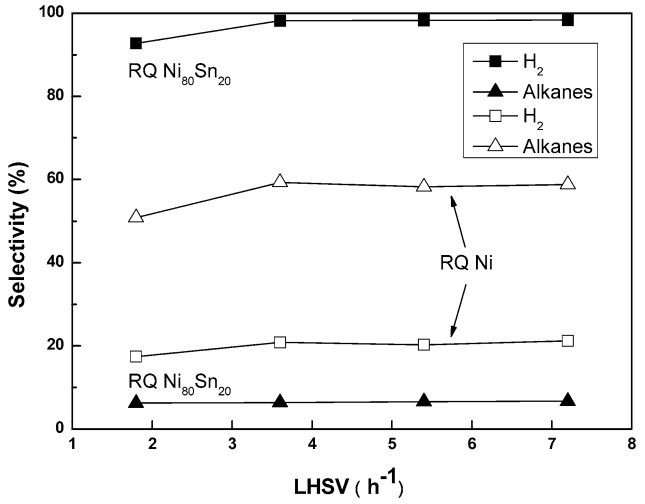

Fig. 8. Effect of LHSV on H_2 and alkane selectivities over the RQ Ni and RQ $Ni_{80}Sn_{20}$ catalysts in APR of ethylene glycol. Other reaction conditions: 0.5 g of catalyst, 5 wt% of ethylene glycol aqueous solution, temperature of 538 K, and pressure of 5.13 MPa. Conversion is above 87% for all points.

under high pressure. In contrast, the activities of the catalysts decreased with rising pressure, in line with the behavior of the Raney Ni–Sn catalysts; Shabaker et al. [7] linked this effect to inhibition by high product partial pressures and reactor dynamics.

Fig. 8 shows the influence of the space velocity of ethylene glycol on the H_2 and alkane selectivities over the RQ Ni and RQ $Ni_{80}Sn_{20}$ catalysts. The reaction temperature and the pressure were fixed at 538 K and 5.13 MPa. It was found that the H_2 and alkane selectivities were affected less by the space velocity of the feed than by the pressure. Moreover, the decreased space velocity or longer residence time did not lead to increased alkane selectivity, as was observed on Raney Ni–Sn [10]. Analysis of the liquid products reveals that the decrease in the H_2 selectivity on RQ $Ni_{80}Sn_{20}$ is due to the formation of more alcohols. Figs. 7 and 8 clearly demonstrate that pressure and space velocity have a lower affect on the H_2 selectivity for the RQ $Ni_{80}Sn_{20}$ catalyst than for the R-$Ni_{14}Sn$ catalyst [10], suggesting that the formation of methane from CO_2 and H_2 is less favorable on RQ $Ni_{80}Sn_{20}$.

4. Discussion

Referring to the reaction pathways outlined by Cortright et al. [5] for the reaction of ethylene glycol with water, C–O cleavage is responsible for the formation of ethanol, whereas the dehydrogenation/rearrangement pathway leads to the formation of organic acids and aldehydes. According to Table 3, the distribution of the liquid products readily rules out the presence of the undesired dehydrogenation/rearrangement pathway on RQ Ni. Moreover, the high methanol/ethanol ratio strongly suggests that C–O cleavage in ethylene glycol was virtually absent on RQ Ni. It is not surprising that RQ Ni exhibited lower activity toward C–O cleavage. We recently found that the temperature required to break the C–S bond in thiophene was about 100 K higher on RQ Ni than on Raney Ni [36].

Based on the XRD results, we tentatively attribute the differences in the catalytic behaviors of RQ Ni and Raney Ni in APR of ethylene glycol to their structure differences due to lattice expansion. The expanded lattice of the RQ Ni catalyst can be expected to affect the reaction pathways of ethylene glycol, thus altering the distributions of the gas and liquid products.

The higher alkane selectivity on RQ Ni can also be explained in light of lattice expansion. For simplicity, we confine our discussion to the formation of methane, which is the main alkanic product (see Table 3). Experimental and theoretical work has demonstrated that CO dissociation on Ni is the rate-determining step for the methanation reaction, $CO + 3H_2 \rightarrow CH_4 + H_2O$ [37–41]. Based on self-consistent density functional calculations, Mavrikakis et al. identified that when the lattice constant parallel to the surface of Ru(0001) is increased or the coordination number is smaller, the d states have to increase in energy, leading to stronger interaction with CO and a lowered dissociation barrier of CO [42]. The correlation between the interaction strength and the d-band center can be generalized to other adsorbates and metals. Because the lattice of RQ Ni is expanded relative to that of Raney Ni, we expect the dissociation probability of CO on RQ Ni to be enhanced, favoring the methanation reaction. Although it may be argued that the enhanced interaction of CO with Ni will also promote the WGS reaction, $CO + H_2O \rightarrow CO_2 + H_2$, which competes for CO and improves H_2 production, Vannice [43] found that the optimum metal–CO interaction required for maximum WGS activity is weaker than the methanation reaction. Thus, H_2 selectivity is lower and alkane selectivity higher on RQ Ni than on Raney Ni.

It is interesting to note that on going from left to right and from 3d to 5d in the periodic table of transition-metal elements, dissociative adsorption of CO is generally suppressed [44]. Dissociative adsorption of CO is observed at high surface temperatures on Ni surfaces, but not on Pt surfaces. This trend is consistent with the finding that Pt is more favorable than Ni in the APR of ethylene glycol to H_2 [8,13], further proving the validity of our understanding of the effect of lattice expansion on the reforming behavior of RQ Ni.

The effect of Sn on H_2 selectivity over the Sn-modified Raney Ni catalysts has been revealed and discussed in the pioneering work of Dumesic and coworkers [9–12]. These authors have suggested that Sn may geometrically modify the catalytic behavior of Ni by preferentially occupying the active sites for CO adsorption and/or dissociation, or by destroying the surface ensembles composed of multiple Ni atoms necessary for CO dissociation [10], thus resulting in higher H_2 selectivity and lower alkane selectivity on the Raney Ni–Sn catalysts.

Because over the RQ Ni and RQ Ni–Sn catalysts the conversions of ethylene glycol to gas products are always >92%, and the liquid products only contains small portion of unreacted feed and <5% of byproducts in carbon under the reaction conditions specified in Fig. 5, the reaction pathways of APR of ethylene glycol can be reasonably simplified as Scheme 1, which involves C–C cleavage, the methanation reaction, and the WGS reaction. Competition between the methanation and the WGS reactions determines the H_2 selectivity. According to the evolution of the TOFs of H_2 and alkanes in Table 4, the above

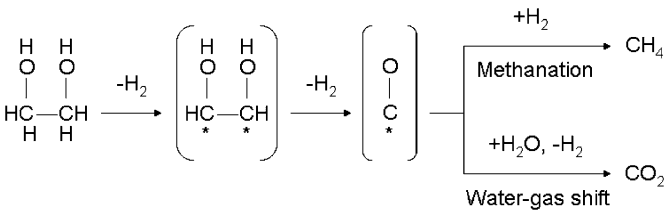

Scheme 1. Simplified reaction pathway for APR of ethylene glycol on the RQ Ni and RQ Ni–Sn catalysts.

interpretations on Sn by Dumesic et al. can be directly adopted to account for the positive role of Sn in the RQ Ni–Sn catalysts. On the other hand, Onda et al. [16] found that on increasing the Sn content in the Ni–Sn intermetallic compounds, the density of state at Fermi level decreased, the width of the Ni 3d peak narrowed, and the peak top of Ni 3d shifted toward higher BE. We expect that such an electronic effect may be operative to a greater or lesser extent on the RQ Ni–Sn catalysts, weakening the bonding of CO [42] and consequently suppressing the methanation reaction. The shift of the high-temperature H_2 desorption peak to lower temperature after Sn addition shown in Fig. 4 also can be rationalized within this framework. In addition, it has been reported that on a PtRu or Pt_3Sn alloy surface, the alloying Ru or Sn is much better than Pt at dissociating H_2O and providing OH groups to react with the CO at Pt sites, which thus promotes the electrochemical oxidation of CO on Pt [45, 46]. We suggest that Sn in the RQ Ni–Sn catalysts may play a role similar to that of Sn in the Pt_3Sn alloy, functioning as an reactive center for H_2O activation. Once the surface OH group is formed on Sn, it readily oxidizes the CO adsorbed on neighboring Ni sites, thus facilitating the WGS reaction and leading to higher H_2 selectivity. This interpretation is compatible with the observation that the TOFs of H_2 and CO_2 increased concomitantly with the addition of Sn (see Table 4).

5. Conclusion

Skeletal Ni catalyst prepared from a rapidly quenched $Ni_{50}Al_{50}$ alloy is intrinsically less selective in producing H_2 but more selective in producing alkanes than Raney Ni in the aqueous-phase reforming of ethylene glycol. This effect is attributed to the expanded lattice of RQ Ni in favor of the dissociation of CO and consequently the methanation reaction, which consumes H_2. Inspection of the gas and liquid products on RQ Ni suggests that the change in the lattice constant influences the reaction pathways of ethylene glycol with H_2O, with complete suppression of the undesired C–O cleavage pathway. Modification of RQ Ni with Sn by simply impregnating RQ Ni in $SnCl_4$ ethanolic solution drastically improves H_2 selectivity. Moreover, H_2 selectivity over the RQ $Ni_{80}Sn_{20}$ catalyst is not sensitive to system pressure and space velocity. Based on our characterizations and previous findings, we suggest that Sn may block the active sites for CO adsorption and/or dissociation, thus suppressing the undesired methanation reaction. On the other hand, the water–gas shift reaction is promoted, most likely due to the activation of H_2O by Sn.

Acknowledgments

This work was supported by Fok Ying Tong Education Foundation (grant 104022), the National Science Foundation of China (grant 20421303), and Shanghai Science and Technology Committee (grant 03QB14004).

References

[1] S.H. Clarke, A.L. Dicks, K. Pointon, T.A. Smith, A. Swann, Catal. Today 38 (1997) 411.
[2] L.K. Rath, J.R. Longanbach, Energy Sources 13 (1991) 443.
[3] J.R. Rostrup-Nielsen, Steam Reforming Catalysts, Danish Technical Press, Copenhagen, 1975.
[4] J.R. Rostrup-Nielsen, Phys. Chem. Chem. Phys. 3 (2001) 283.
[5] R.D. Cortright, R.R. Davda, J.A. Dumesic, Nature 418 (2002) 964.
[6] J.W. Shabaker, G.W. Huber, R.R. Davda, R.D. Cortright, J.A. Dumesic, Catal. Lett. 88 (2003) 1.
[7] J.W. Shabaker, R.R. Davda, G.W. Huber, R.D. Cortright, J.A. Dumesic, J. Catal. 215 (2003) 344.
[8] R.R. Davda, J.W. Shabaker, G.W. Huber, R.D. Cortright, J.A. Dumesic, Appl. Catal. B 43 (2003) 13.
[9] G.W. Huber, J.W. Shabaker, J.A. Dumesic, Science 300 (2003) 2075.
[10] J.W. Shabaker, G.W. Huber, J.A. Dumesic, J. Catal. 222 (2004) 180.
[11] J.W. Shabaker, J.A. Dumesic, Ind. Eng. Chem. Res. 43 (2004) 3105.
[12] J.W. Shabaker, D.A. Simonetti, R.D. Cortright, J.A. Dumesic, J. Catal. 231 (2005) 67.
[13] R.R. Davda, J.W. Shabaker, G.W. Huber, R.D. Cortright, J.A. Dumesic, Appl. Catal. B 56 (2005) 171.
[14] D.A. Morgenstern, J.P. Fornango, Energy Fuels 19 (2005) 1708.
[15] H.R. Hu, M.H. Qiao, Y. Pei, K.N. Fan, H.X. Li, B.N. Zong, X.X. Zhang, J. Catal. 221 (2004) 612.
[16] A. Onda, T. Komatsu, T. Yashima, Phys. Chem. Chem. Phys. 2 (2000) 2999.
[17] A. Onda, T. Komatsu, T. Yashima, J. Catal. 201 (2001) 13.
[18] A. Onda, T. Komatsu, T. Yashima, J. Catal. 221 (2003) 378.
[19] P. Gallezot, P.J. Cerino, B. Blanc, G. Flèche, P. Fuertes, J. Catal. 146 (1994) 93.
[20] P. Lesage, O. Clause, P. Moral, B. Didillon, J.P. Candy, J.M. Basset, J. Catal. 155 (1995) 238.
[21] N.N. Nichio, M.L. Casella, G.F. Santori, E.N. Ponzi, O.A. Ferretti, Catal. Today 62 (2000) 231.
[22] PDFMaint Version 3.0, Powder Diffraction Database, Bruker Analytical X-Ray Systems GmbH, 1997.
[23] H.E. Swanson, E. Fuyat, Natl. Bur. Stand. Circ. 1 (1953) 13.
[24] S.D. Robertson, R.B. Anderson, J. Catal. 23 (1971) 286.
[25] J. Wintterlin, T. Zambelli, J. Trost, J. Greeley, M. Mavrikakis, Angew. Chem. Int. Ed. 42 (2003) 2850.
[26] J.F. Moulder, W.F. Stickle, P.E. Sobol, K.D. Bomben, in: J. Chastain (Ed.), Handbook of X-Ray Photoelectron Spectroscopy, Perkin–Elmer, Eden Prairie, MN, 1992.
[27] P. Fouilloux, Appl. Catal. 8 (1983) 1.
[28] F. Delannay, J.P. Damon, J. Masson, B. Delmon, Appl. Catal. 4 (1982) 169.
[29] C. Padeste, D.L. Trimm, Catal. Lett. 17 (1993) 333.
[30] K. Christmann, O. Schober, G. Ertl, M. Neumann, J. Chem. Phys. 60 (1974) 4528.
[31] M. Arai, K. Suzuki, Y. Nishiyama, Bull. Chem. Soc. Jpn. 66 (1993) 40.
[32] J. Greeley, W.P. Krekelberg, M. Mavrikakis, Angew. Chem. Int. Ed. 43 (2004) 4296.
[33] R.A. Lemons, J. Power Sources 29 (1990) 251.
[34] L.J. Shorthouse, A.J. Roberts, R. Raval, Surf. Sci. 480 (2001) 37.
[35] R.M. Koros, E.J. Nowak, Chem. Eng. Sci. 22 (1967) 470.
[36] H.R. Hu, M.H. Qiao, F.Z. Xie, K.N. Fan, H. Lei, D.L. Tan, X.H. Bao, H.L. Lin, B.N. Zong, X.X. Zhang, J. Phys. Chem. B 109 (2005) 5186.
[37] D.W. Goodmann, R.D. Kelley, T.E. Madey, J.M. White, J. Catal. 64 (1980) 479.

[38] A.T. Bell, Catal. Rev. Sci. Eng. 23 (1981) 203.
[39] J.W.E. Coenen, P.F.M.T. van Nisselroy, M.H.J.M. de Croon, P.F.H.A. van Dooren, R.Z.C. van Meerten, Appl. Catal. 25 (1986) 1.
[40] H.S. Bengaard, J.K. Nørskov, J. Sehested, B.S. Clausen, L.P. Nielsen, A.M. Molenbrock, J.R. Rostrup-Nielsen, J. Catal. 209 (2002) 365.
[41] J. Sehested, S. Dahl, J. Jacobsen, J.R. Rostrup-Nielsen, J. Phys. Chem. B 109 (2005) 2432.
[42] M. Mavrikakis, B. Hammer, J.K. Nørskov, Phys. Rev. Lett. 81 (1998) 2819.
[43] M.A. Vannice, J. Catal. 50 (1977) 228.
[44] R.I. Masel, Principles of Adsorption and Reaction on Solid Surfaces, Interscience, New York, 1996.
[45] P. Liu, A. Logadottir, J.K. Nørskov, Electrochim. Acta 48 (2003) 3731.
[46] M.T.M. Koper, Surf. Sci. 548 (2004) 1.